Radiocarbon, Vol 57, Nr 1, 2015, p 109–122 DOI: 10.2458/azu_rc.57.18118

ULTRA-SMALL GRAPHITIZATION REACTORS FOR ULTRA-MICROSCALE ^{14}C ANALYSIS AT THE NATIONAL OCEAN SCIENCES ACCELERATOR MASS SPECTROMETRY (NOSAMS) FACILITY

Sunita R Shah Walter[1] • Alan R Gagnon • Mark L Roberts • Ann P McNichol • Mary C Lardie Gaylord • Elizabeth Klein

Geology and Geophysics Department, Woods Hole Oceanographic Institution, 360 Woods Hole Road, Woods Hole, MA 02543, USA.

ABSTRACT. In response to the increasing demand for ^{14}C analysis of samples containing less than 25 µg C, ultra-small graphitization reactors with an internal volume of ~0.8 mL were developed at NOSAMS. For samples containing 6 to 25 µg C, these reactors convert CO_2 to graphitic carbon in approximately 30 min. Although we continue to refine reaction conditions to improve yield, the reactors produce graphite targets that are successfully measured by AMS. Graphite targets produced with the ultra-small reactors are measured by using the Cs sputter source on the CFAMS instrument at NOSAMS where beam current was proportional to sample mass. We investigated the contribution of blank carbon from the ultra-small reactors and estimate it to be 0.3 ± 0.1 µg C with an Fm value of 0.43 ± 0.3. We also describe equations for blank correction and propagation of error associated with this correction. With a few exceptions for samples in the range of 6 to 7 µg C, we show that corrected Fm values agree with expected Fm values within uncertainty for samples containing 6–100 µg C.

INTRODUCTION

Demand for radiocarbon analysis of samples containing less than 25 micrograms of carbon (µg C) has increased in recent years with the development and proliferation of new methods to isolate specific compounds from environmental samples for ^{14}C analysis (e.g. Ohkouchi et al. 2005; Ingalls et al. 2006, 2010; Ziolkowski and Druffel 2009). While compound-specific ^{14}C analysis (CSRA) studies often result in small quantities of purified compound, even from large quantities of bulk sediments or filtered seawater (Shah and Pearson 2007; Santos et al. 2010), they have proven to be useful for identifying individual sources in heterogeneous sedimentary organic matter (Ohkouchi et al. 2002; Drenzek et al. 2007) and constraining the carbon sources and metabolisms of marine microbial groups *in situ* (Pearson et al. 2005; Ingalls et al. 2006). The capability to measure samples containing less than 25 µg C samples will also facilitate the ^{14}C analysis of small numbers of individual foraminiferal shells, allowing for more detailed investigations of heterogeneity in their ^{14}C ages in sediment (e.g. Keigwin and Guilderson 2009), and it will allow for the ^{14}C analysis of finer fractions of volatiles and CO_2 evolved during ramped pyrolysis experiments (e.g. Rosenheim et al. 2008; Rosenheim and Galy 2012).

Currently at the National Ocean Sciences Accelerator Mass Spectrometry (NOSAMS) Facility, three graphite production vacuum systems convert CO_2 from samples of unknown age and standards to graphite targets for AMS analysis. These vacuum systems are compatible with two types of graphitization reactor: reactors constructed with 9-mm-diameter tubing and a nominal internal volume of 11 mL, used for samples containing 100 to 4000 µg C, and 6-mm reactors with a nominal internal volume 3.5 mL, used for samples containing 25 to 1500 µg C (Pearson et al. 1998; Gagnon et al. 2000). For routine ^{14}C analysis, the minimum sample size limit at NOSAMS has been 25 µg C (Pearson et al. 1998). This article describes the design and performance of new ultra-small volume graphitization reactors for samples in the range of 6–100 µg C. We also quantify the mass of contaminant carbon added by the ultra-small reactors, discuss its subtraction from measured fraction modern (Fm) values, and discuss the propagation of uncertainty associated with this subtraction. CSRA is limited to samples containing greater than 5 or 10 µg C because typically between 1 and 5 µg C of contaminant carbon is incorporated in these samples from isolation and purification procedures (Shah and Pearson 2007; Santos et al. 2010). Considering the limits imposed by contaminant carbon, the mass range of these reactors is compatible with the smallest compound-specific samples.

1. Corresponding author. Email: shah@fas.harvard.edu.

REACTOR DESCRIPTION, OPERATION, AND YIELD

At NOSAMS, H_2 and CO_2 are reduced to graphitic carbon and water over a catalyst of reduced iron powder in reactors constructed from Ultra-Torr tee fittings (Pearson et al. 1998). Each tee is fitted with one quartz tube containing the catalyst and one Pyrex® tube, which serves as a cold trap to capture water vapor. Pressure transducers are mounted onto the tee fitting to monitor the progress of the reaction. The reactors are connected to a vacuum line through a tube welded to the tee body and an automated pneumatic valve. Custom-developed LabVIEW programs control the pneumatic valves and ovens and monitor the pressure transducers (Gagnon et al. 2000). A proven approach to graphitizing smaller samples while minimizing isotopic fractionation has been to reduce the internal volume of reactors (Pearson et al. 1998; Santos et al. 2007; Yokoyama et al. 2010). For ultra-microscale samples (<25 µg C), this has been accomplished by miniaturizing the tee body and shortening tube lengths while maintaining modularity by keeping tube outer diameter constant (Santos et al. 2007), or by precision-machining reactors with narrow internal diameters (Liebl et al. 2010). Our approach was a hybrid, reducing tube outer diameters to 3.2 mm while constructing the reactors from commercially available parts, analogous to our larger-volume reactors.

Ultra-small reactors were assembled from 1/8″ stainless steel Ultra-Torr tee fittings to which a 1/8″ Swagelok tube adapter was silver-soldered to make a cross (Figure 1). A 1/8″ Swagelok plug valve was fitted onto the tube adapter that connects the reactor to the vacuum line. Inexpensive Omega PX-139 Series pressure transducers were modified to be compatible with the 1/8″ Ultra-Torr fittings and reactor pressures are displayed and recorded by a LabVIEW program through an HP 3852A Data Acquisition/Control Unit. With the Swagelok plug valves and control of the ultra-small ovens achieved by an Omega CN76000 AutoTune PID controller, operation of the ultra-small reactors is largely manual compared to other graphite systems at NOSAMS. Graphitic carbon is produced over 2.5 mg of Mallinckrodt 325-mesh reduced iron catalyst in a 3.2 mm OD × 2.0 mm ID × 30 mm quartz tube. Water produced during the CO_2 reduction reaction is trapped cryogenically in a Pyrex tube of the same dimensions immersed in a slurry of dry ice and isopropanol. The internal volume of our reactors is approximately 0.8 mL. Four reactors are mounted to the vacuum line and up to 12 targets can be produced per day. Targets are stored in an Ar atmosphere until pressing, which typically occurs within two weeks.

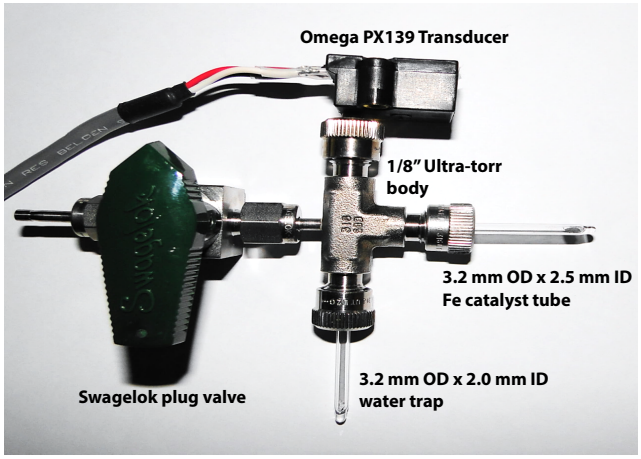

Figure 1 Ultra-small volume reactors

Ovens were custom fabricated and optimized to evenly heat narrow-diameter reactor tubes. Prior to use, iron catalyst is prebaked in the reactors under 1 atmosphere of H_2 gas at 425°C for 40 min.

In situ hydrogen baking is followed by baking at 625°C for 15 min under vacuum. We found that avoiding transfer of CO_2 through multipurpose vacuum lines both reduced CO_2 loss and reduced process blank. Sample CO_2 is loaded into the reactors directly from small-volume resealable finger flasks (Figure 2). Both finger flasks and graphite reactors are mounted on a vacuum line port by a 1/4″ Ultra-Torr tee fitting so that the internal space of the tee fitting can be pumped out prior to the transfer of sample CO_2 from the finger flask to the reactor (Figure 2). For different types of samples, the finger flasks can be replaced by a tube cracker or hydrolysis reactor. Following H_2 addition to the reactors in a H_2/CO_2 ratio of approximately 2.5, the reaction proceeds at 625°C (McNichol et al. 1992). By monitoring the reactor pressure, we observe that the reaction generally completes within 30 min for samples up to 25 µg C. Yields above 90% are calculated from pressures and reaction stoichiometry (Osborne et al. 2000), although the smallest samples (<10 µg C) yield pressures that are close to the uncertainty limit of our transducers. For example, 6 µg C of CO_2 yields a pressure of approximately 0.2 ± 0.15 psi.

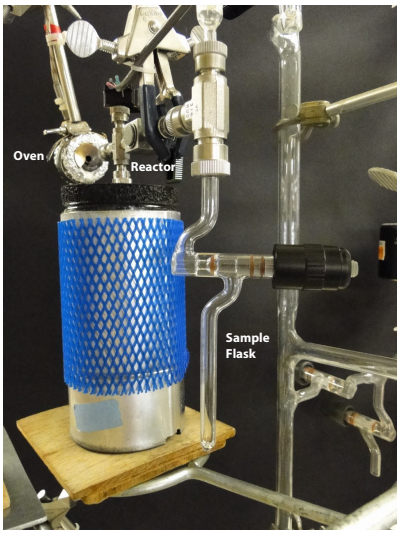

Figure 2 Reactors on vacuum line with ovens and sample flask

PREPARATION OF STANDARDS

One of our goals was to investigate the addition of exogenous carbon during the process of converting CO_2 to graphite using the ultra-small reactors. In order to minimize blank contributions from other preparative procedures (i.e. combustion of organic compounds and acid hydrolysis of carbonates to CO_2), all standards were prepared in large batches (280–36,000 µg C). This strategy allows combustion or hydrolysis blanks to be diluted over a large sample mass, thereby minimizing the proportion of process blank in smaller CO_2 splits (Vogel et al. 1987). Process blanks specific to the NOSAMS sample preparation lab for large-mass samples (Table 1) are much smaller than batches of secondary standards (≥300 µg C).

Table 1 Blanks associated with sample preparation processes at NOSAMS.

Sample type	Process description	Blank mass (µg C)	Blank Fm value
inorganic	acid hydrolysis	0.3 ± 0.1	0.8 ± 0.3
organic	combustion by elemental analyzer	1.2 ± 0.5	0.5 ± 0.3
organic	closed-tube combustion	1.2 ± 0.6	0.25 ± 0.03

The modern primary standard, NIST HOx-I (Fm ≡ 1/0.95; Stuiver and Polach 1977; Currie and Polach 1980) was prepared as large-mass bulb combustions or by combustion via elemental analyzer in the NOSAMS sample preparation lab. IAEA C-1 (Fm = 0.0002 ± 0.002) (Rozanski et al. 1992) was prepared by H_3PO_4 hydrolysis in batches of 2.2–2.6 mg C. Organic secondary standards were also combusted by a Costech 4010 elemental analyzer in batches of ~0.3 mg C: HOx-II ($Fm_{HOx\text{-}II}$/ $Fm_{HOx\text{-}I}$ = 1.2933 ± 0.0004) (Mann 1983; Stuiver 1983), FIRI-H wood (Fm = 0.7574 ± 0.0004) (Scott 2003), IAEA C-7 (Fm = 0.4953 ± 0.0012) (Le Clercq et al. 1998), IAEA C-8 (Fm = 0.1503 ± 0.0017) (Le Clercq et al. 1998), and acetanilide (Baker part A068-03, Lot #V44467). Acetanilide is an internal standard with an Fm value indistinguishable from other "dead" organic secondary standards (e.g. anthracite, old wood) and is the routine process blank material used at NOSAMS for organic carbon combustions.

From large standard preparations, smaller aliquots of CO_2 were split immediately before graphitization on the NOSAMS vacuum line designed to accurately quantify samples as small as 1.0 µg C. This vacuum line is equipped with a 10-torr MKS capacitance manometer that measures pressure in a volume of 16.5 ± 0.9 mL, yielding an overall mass uncertainty of 5.4–6.2%. The measured volume can also be expanded via a glass barrel valve to 133 ± 7 mL for quantification of samples up to 850 µg C.

A close examination of ^{14}C results from organic and inorganic "dead" standards (Fm = 0), acetanilide and IAEA C-1, convinces us that this strategy of processing large samples followed by splitting into smaller CO_2 aliquots was successful. The results are consistent with a single, small-mass process blank that represents the graphitization process. Assuming the measured sample is composed of CO_2 from the standard plus a constant-mass process blank representing the cumulative contaminant from all preparative steps, the mass and fraction modern of the measured sample can be represented as

$$m_{meas} = m_{std} + m_{pb} \tag{1}$$

and

$$Fm_{meas} = \frac{m_{std} * Fm_{std} + m_{pb} * Fm_{pb}}{m_{meas}} \tag{2}$$

where m_{meas} is the carbon mass of the measured sample, m_{pb} the mass of the process blank, and m_{std} the mass of the standard. Fm_{meas}, Fm_{pb}, and Fm_{std} are the corresponding fractions modern. Substituting Equation 1 into Equation 2 and re-arranging to the equation of a line where y is Fm_{meas} and x is the inverse of m_{meas} allows for a constant mass blank to be described by a linear relationship. Figure 3 illustrates that all "dead" standards do indeed fall on a single line, implying a common process blank.

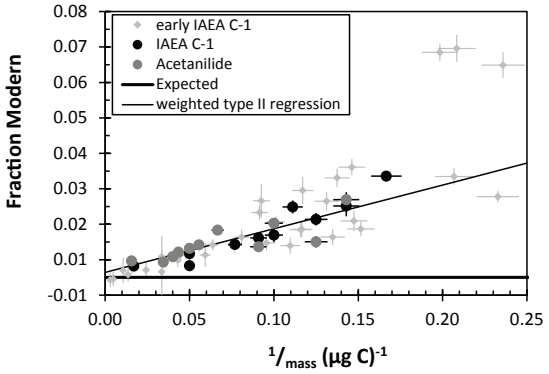

Figure 3 Fm values for ultra-small "dead" targets from CFAMS041513 and CFAMS071613, normalized to 1 mg C HOx-I standards, are plotted as large black or dark gray circles against inverse mass along with their uncertainty-weighted Type II regression line. Fm values from four previous wheels, which had graphite targets produced under varying graphitization conditions (early IAEA C-1), are also plotted as small, light gray diamonds. The expected Fm value of 0.0 is included as the thick black line.

ISOTOPIC FRACTIONATION

To determine the magnitude of fractionation introduced by the ultra-small reactors, graphite was produced from HOx-I, IAEA C-6 (Rozanski et al. 1992), IAEA C-2 (Rozanski et al. 1992), and IAEA C-1 standards, spanning a range of $\delta^{13}C$ values, then subsequently combusted back to CO_2 by elemental analyzer. The $\delta^{13}C$ value of the resulting CO_2 was measured by a dual-inlet isotope-ratio mass spectrometer. As reported by other AMS facilities (van der Borg et al. 1997; Hua et al. 2001; Santos et al. 2007), there appears to be a significant isotopic fractionation associated with the graphitization of ultra-microscale samples. Figure 4 illustrates the apparent mass dependence of this fractionation effect for our ultra-small reactors. Our reactors and reaction conditions result in a somewhat larger fractionation than observed by Santos et al. (2007), who were able to minimize isotopic fractionation and achieve nearly 100% yield by optimizing reaction temperature. The fractionation observed suggests that the reactions are not going to completion for our smallest samples. Although our pressure transducers indicate we obtain >90% yield, the pressure change seen for samples containing <10 µg C is similar to the reported uncertainty of the transducers. For samples containing ≤10 µg C, up to an 8‰ difference between the measured and expected $\delta^{13}C$ values was observed (Figure 4). If our reactions are not going to completion, then our mass-based process blank corrections are not exact and the smallest samples will be affected the most.

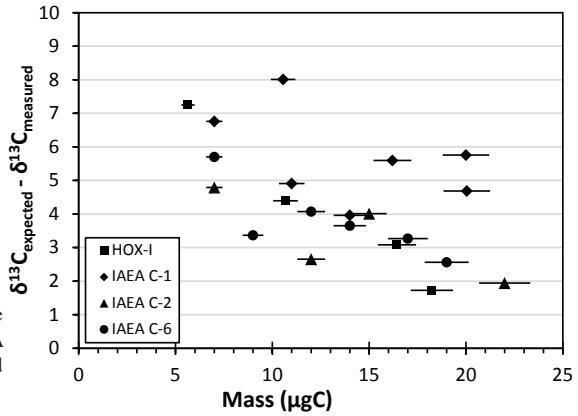

Figure 4 Isotopic fractionation observed from graphite recombustions for HOx-I and secondary standards IAEA C-1, C-2, and C-6. The difference between measured and expected $\delta^{13}C$ values are plotted against sample mass.

Assuming that fractionation in the CO_2 to graphite reaction proceeds according to a Rayleigh distillation, it is possible to estimate the degree of completion of the reaction. Although the conversion of CO_2 to graphite is a sequence of reactions, others have estimated a fractionation factor using the overall reaction and calculated fractionation factors (α) ranging from 0.972 to 0.995 (Kitagawa et al. 1993; Verkouteren et al. 1997; Xu et al. 2007). Figure 5 shows the expected values for $\Delta\delta^{13}C$, the difference between the initial $\delta^{13}C$ value, and the $\delta^{13}C$ value at each point along the progress of the reaction for both CO_2 and graphite with Rayleigh distillation fractionation factors of 0.970 and 0.988. When we conducted a fractionation experiment in 2000, stopping the graphite reaction at various stages of completion (as measured by pressure change) and measuring the $\delta^{13}C$ of the gas remaining in the graphite reactor (Figure 5), our data were consistent with an α value of 0.988. The $\Delta\delta^{13}C$ values observed for recombusted graphite (Figure 4), however, are more consistent with an α value of 0.970. This is likely due to the different reaction conditions for graphite preparation of ultra-small and normal-sized (>500 µg C) samples. Comparing the $\Delta\delta^{13}C$ values measured on recombusted graphite with the solid black line in Figure 5 suggests that the graphite reactions have proceeded to at least 60% completion. It is difficult to say more given the insensitivity of the graphite fractionation at yields >60%. More detailed investigations into the optimal temperature for both maximum yield and minimum isotopic fractionation is the subject of ongoing work at NOSAMS.

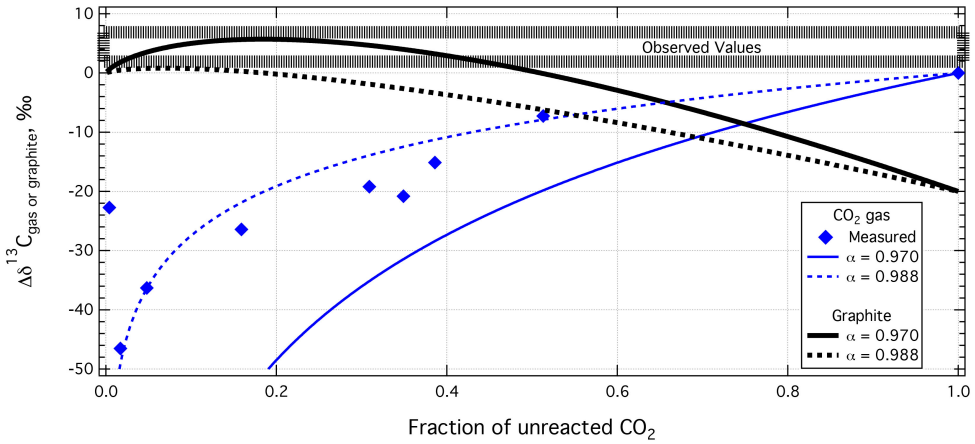

Figure 5 Relationship of $\Delta\delta^{13}C$ to the fraction of unreacted CO_2 in a graphite reactor. The solid blue and black lines reflect the expected values for the CO_2 and graphite, respectively, assuming a Rayleigh fractionation factor, α, of 0.970. The dashed blue and black lines are the same for an α of 0.988. The blue diamonds are CO_2 data from a reaction conducted in 2000 and the black box shows the range of $\Delta\delta^{13}C$ values for ultra-small graphite samples.

BEAM CURRENT YIELD FROM ULTRA-SMALL GRAPHITE TARGETS

All ultra-small graphite targets were measured using the Cs sputter source on the CFAMS instrument at NOSAMS (Roberts et al. 2010). To investigate AMS performance on graphite targets produced with the ultra-small reactors, a large suite of primary and secondary ^{14}C standards spanning a mass range of 6–100 µg C were prepared and measured on a single wheel, CFAMS041513. We do not observe the same rapid collapse in $^{12}C^+$ beam current reported by Santos et al. (2007) and Liebl et al. (2013) with ultra-microscale graphite targets produced on <4 mg of reduced iron catalyst (Figure 6). From our 6 and 25 µg C targets, produced with 2.5 mg of catalyst, we were able to obtain 6–10 individual measurements, each lasting 3 min or 30,000 ^{14}C counts, whichever came first. We generally observe a smaller yield of beam current per microgram of carbon than the 1 µA/µg C reported by other AMS facilities (Santos et al. 2007; Liebl et al. 2013) as well as variability in the beam current yield from wheels measured on different days (Figure 6).

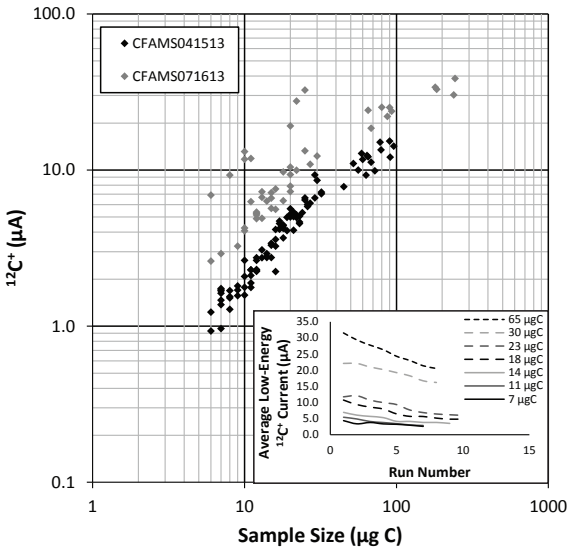

Figure 6 Maximum $^{12}C^+$ beam current for primary and secondary standards with 6–100 µg of carbon from wheels CFAMS041513 and CFAMS071613. Inset plot shows average low-energy $^{12}C^+$ current for a series of individual measurements from the same target. All targets were produced from HOx-I with a range of masses.

^{14}C RESULTS AND BLANK DETERMINATION

Fraction modern results for wheels CFAMS041513 and CFAMS071613 are reported in the Appendix. These wheels as well as four previous wheels that were measured as we optimized parameters such as oven design, quantity of iron catalyst, CO_2/H_2 ratio, and method of CO_2 introduction are summarized in Figures 3 and 7 for ^{14}C-dead standards and primary standard HOx-I, respectively. Despite changing reaction conditions, all six wheels show remarkable consistency in the relationship between the Fm value of "dead" standards and inverse sample mass (Figure 3). Still, we only use results from CFAMS041513 and CFAMS071613 (black and dark gray circles) to calculate and correct for the exogenous carbon added by the ultra-small reactors. All results plotted in Figures 3 and 7 are corrected for machine-induced isotopic fractionation by the online ^{13}C measurement (Santos et al. 2007), normalized to large (~1 mg C) HOx-I standards and corrected for AMS background based on unprocessed Alfa Aesar graphite targets (Alfa Aesar graphite powder, ultra superior, –200 mesh, 99.9999% pure; lot #H24F24). The background measurement for both CFAMS041513 and CFAMS071613 combined was Fm = 0.0010.

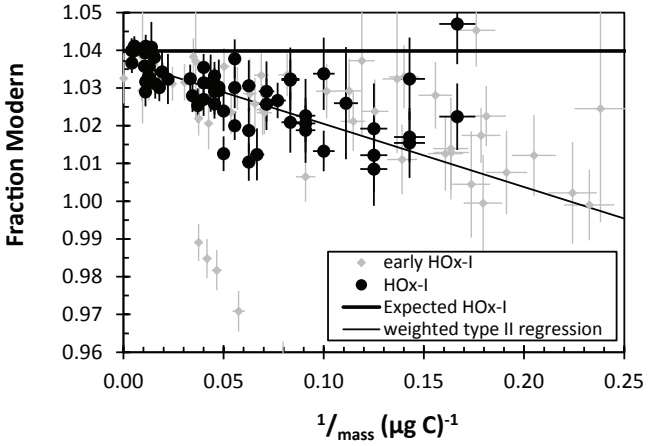

Figure 7 Fm values for ultra-small HOx-I targets from CFAMS041513 and CFAMS071613, normalized to 1 mg C HOx-I standards, are plotted as large black circles against inverse mass along with their uncertainty-weighted Type II regression line. Fm values from four previous wheels that had graphite targets produced under varying graphitization conditions (early HOx-I) are also plotted as small, light gray diamonds. The expected Fm value of 1.0398 is included as the thick black line.

For both modern and dead standards, our measured Fm values show clear mass dependence such that smaller sample sizes deviate more from expected Fm values than larger sizes (Figures 3 and 7). Having corrected for AMS background and minimized the contributions of blank carbon from sample combustion or carbonate hydrolysis to CO_2, this is likely to result from a constant mass of contaminant carbon added during the graphitization process (Vogel et al. 1987). Corrections for process blank have generally followed one of two approaches: (1) normalizing unknowns using size-matched standards or (2) correction for process blank by mass balance. We compared normalization of ultra-microscale samples to HOx-I standards in the range of 60 to 100 µg C to correction by mass-balance subtraction of the graphitization blank. The residual difference between expected and corrected Fm values for the two methods is illustrated in Figure 8. Both approaches yield similar results, although the average residual for mass-balance correction (0.0058) is smaller than the average for normalization to 60–100 µg C HOx-I standards (0.0070). For this reason, we describe our estimation of graphitization blank below and employ mass-balance correction for the large suite of primary and secondary standards measured on CFAMS041513 and CFAMS071613 (Figures 9a and 9b). However, as the difference is small, the comparison between mass-balance correction and normalization to small standards will be continually re-evaluated as more ultra-small targets are measured over time at NOSAMS.

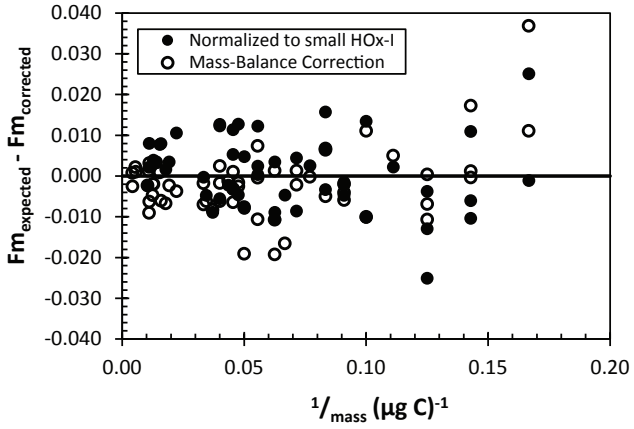

Figure 8 Comparison of correction methods for ultra-small HOx-I graphite targets from CFAMS041513 and CFAMS071613. Difference between expected and corrected or normalized Fm values are plotted against inverse sample mass with normalized results in solid circles and results corrected by mass-balance subtraction of blank in open circles.

To determine the magnitude of the process blank, we follow the approach outlined in Santos et al. (2007) of separately calculating modern and dead components assuming the blank and standards are linearly additive according to the following mass balance equations:

$$m_{meas} = m_{std} + m_{b\_modern} + m_{b\_dead} \tag{3}$$

and

$$Fm_{meas} = \frac{m_{std} * Fm_{std} + m_{b\_modern} * Fm_{b\_modern} + m_{b\_dead} * Fm_{b\_dead}}{m_{meas}} \tag{4}$$

where we have substituted m_{b_modern} and m_{b_dead} for the total process blank (m_{pb}) in Equations 1 and 2 above. For mathematical convenience, we assign the Fm of the modern blank component (Fm_{b_modern}) to 1.0 and $Fm_{b\_dead} \equiv 0.0$.

The modern component of the graphitization blank was determined using ^{14}C-dead standards: IAEA C-1 and acetanilide. In this case, where $Fm_{std} = 0$, the equations described above can be simplified to

$$Fm_{meas} = \frac{m_{b\_modern}}{m_{meas}} \tag{5}$$

an expression that can be viewed as an equation of a line of the form $y = mx + b$, where y is Fm_{meas}, x is $^1/m_{meas}$, and the slope is the mass of the modern blank (Figure 3). The y intercept, representing Fm_{std}, is expected to be 0. An uncertainty-weighted Type II regression was calculated by the MATLAB routine lsqcubic.m (E T Peltzer, http://www.mbari.org/staff/etp3/regress.htm, accessed August 2013). The regression line has an R^2 value of 0.89 and a y intercept, or modeled Fm_{std}, of 0.0014. This estimate of Fm_{std} is within measurement uncertainty of large IAEA C-1 targets on the same wheels, giving confidence to the model described by Equation 5. Calculating the mass of the modern blank (slope) yields a value of 0.12 µg C. Considering that R^2 represents the fraction of variability accounted for by our regression line, we assign the uncertainty as $(1 - R^2) * m_{b\_modern}$, or 0.01 µg C (Table 2).

Table 2 Graphitization blanks for ultra-small reactors.

	Blank mass (µg C)	Blank Fm value
Individually calculated blank components		
Modern	0.12 ± 0.01	1.0
Dead	0.2 ± 0.1	0.0
Combined graphitization blank		
Total	0.28 ± 0.1	0.43 ± 0.3

By analogous methods, we determine the "dead" component of the graphitization blank from the ^{14}C results from HOx-I standards. With $Fm_{std} = Fm_{HOx\text{-}I}$, Equation 4 reduces to

$$Fm_{meas} = \frac{m_{b\_modern} * \left(1 - Fm_{HOx\text{-}I}\right) - m_{b\_dead} * Fm_{HOx\text{-}I}}{m_{meas}} + Fm_{HOx\text{-}I} \tag{6}$$

In this expression, the mass of the dead blank (m_{b_dead}) is calculated from the slope of the regression line combined with the values for $Fm_{HOx\text{-}I}$ and m_{b_modern} described above (Table 2). It is calculated according to

$$m_{b\_dead} = \frac{m_{b\_modern} * \left(1 - Fm_{HOx\text{-}I}\right) - \text{slope}}{Fm_{HOx\text{-}I}} \tag{7}$$

The linear model, however, does not fit HOx-I results as well as it does for "dead" standards (Figure 7). The uncertainty-weighted Type II regression yields an R^2 value of only 0.35, although the modeled estimate of $Fm_{HOx\text{-}I}$, or the y intercept, is 1.0372, well within the range of large (1 mg C) HOx-I standards measured on the same two wheels.

The systematic decrease in the Fm value of HOx-I standards with sample mass illustrated in Figure 7 is not specific to the ultra-small reactors at NOSAMS, appearing in <100 µg C HOx-I standards graphitized on the Small Sample Line (Pearson et al. 1998; von Reden et al. 1998) and at other AMS facilities (e.g. Kirner et al. 1995; Santos et al. 2007). While subtraction of a constant-mass process blank has been employed to correct for the anomalously low Fm results in ultra-microscale standards (Vogel et al. 1987; Hua et al. 2004; Santos et al. 2007), other processes have also been invoked to explain this effect (Kirner et al. 1995; von Reden et al. 1998). It is possible that our model, described in Equation 6, does not adequately account for the effects of machine conditions and beam geometry. But because a constant-mass "dead" blank is likely to contribute to the low Fm values seen in small modern standards (Figure 7), and because our model does yield an accurate estimate of the expected $Fm_{HOx\text{-}I}$, we proceed with describing the graphitization blank. From Equation 7 and the slope of the Type II regression line (–0.1672), the mass of the dead component of the graphitization blank is 0.16 µg C. The associated uncertainty is much larger compared to the modern blank due to the poor fit of the linear model to measured HOx-I fractions modern. Using the strategy described above for the modern blank results in an uncertainty estimate of ± 0.10 (Table 2).

Combined, we calculate a total graphitization blank of 0.28 ± 0.1 µg C with Fm = 0.43 ± 0.3, where the uncertainties are determined by summing in quadrature. The large relative uncertainties in these values are driven by the uncertain estimate for m_{b_dead}.

BLANK CORRECTION AND SECONDARY STANDARDS

To test our blank-correction strategy, we applied it to primary and secondary standards measured on test wheels CFAMS041513 and CFAMS071613. As described previously, our preparation method was designed to make the graphitization blank prominent while minimizing the contribution of blank carbon from other pretreatment processes. The corrected Fm value was calculated from a re-arrangement of Equation 4:

$$Fm_{std} = \frac{m_{meas} * Fm_{meas} - m_{b\_modern}}{m_{meas} - m_{b\_modern} - m_{b\_dead}} \quad (8)$$

Figures 9a and 9b summarize the ^{14}C data before and after correction for modern and dead components of the graphitization blank. After blank correction, most primary and secondary standards in the ultra-microscale range show significantly greater similarity with their expected Fm values (Figure 9b). Only IAEA C-7 appears to be unaffected by the correction. But as the expected Fm of this standard ($Fm_{IAEA\ C\text{-}7} = 0.4953 \pm 0.0012$) is most similar to the combined Fm of the process blank ($Fm_b = 0.43 \pm 0.3$), a large correction is not expected. The apparent failure of the graphitization blank correction for the smallest (6–7 µg C) samples indicates a possible undercorrection for the modern component of the graphitization blank.

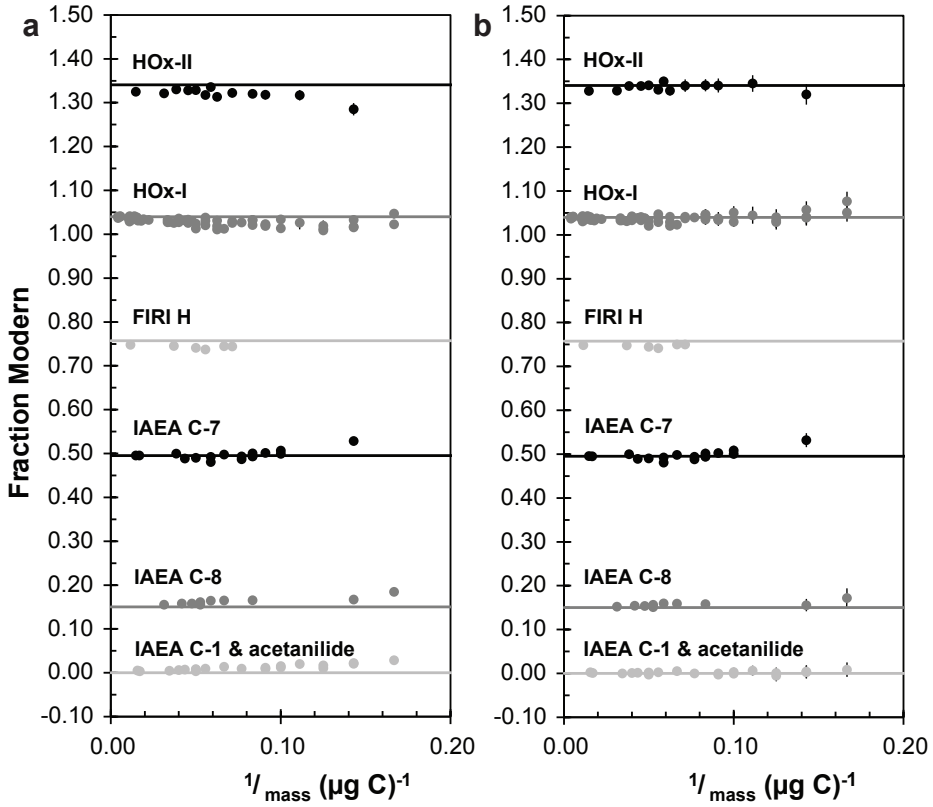

Figure 9 Fractions modern for primary and secondary standards (a) before and (b) after mass-balance correction for graphitization blank.

The propagated uncertainty associated with blank correction is assigned considering that Fm_{std} represents many individual measurements, $Fm_{std,n}$, each of which is a function of $m_{meas,n}$, $Fm_{meas,n}$,

$m_{b\_modern,n}$, and $m_{b\_dead,n}$. The error, therefore, can be represented as a statistical function dependent on N individual differences between $Fm_{std,n}$ and the average value, $\overline{Fm_{std}}$. Assuming small random deviations in $Fm_{meas,n}$ from $\overline{Fm_{meas}}$, $m_{meas,n}$ from $\overline{m_{meas}}$, $m_{b\_modern,n}$ from $\overline{m_{b\_modern}}$, and $m_{b\_dead,n}$ from $\overline{m_{b\_dead}}$ are responsible for the individual deviations between $Fm_{std,n}$ and $\overline{Fm_{std}}$, and following the approach outlined in Shah and Pearson (2007), the variance of Fm_{std} can be written as

$$\sigma^2_{Fm_{std}} = \frac{1}{N}\sum_1^N f\left[\left(Fm_{meas,n} - \overline{Fm_{meas}}\right)\frac{\partial Fm_{std}}{\partial Fm_{meas}} + \left(m_{meas,n} - \overline{m_{meas}}\right)\frac{\partial Fm_{std}}{\partial m_{meas}} + \left(m_{b\_modern,n} - \overline{m_{b\_modern}}\right)\frac{\partial Fm_{std}}{\partial m_{b\_modern}} + \left(m_{b\_dead,n} - \overline{m_{b\_dead}}\right)\frac{\partial Fm_{std}}{\partial m_{b\_dead}}\right]^2 \quad (9)$$

Expanding this function as a Taylor series, keeping only the first-order terms, results in

$$\sigma^2_{Fm_{std}} = \frac{1}{N}\sum_1^N f\left[\left(Fm_{meas,n} - \overline{Fm_{meas}}\right)\frac{\partial Fm_{std}}{\partial Fm_{meas}} + \left(m_{meas,n} - \overline{m_{meas}}\right)\frac{\partial Fm_{std}}{\partial m_{meas}} + \left(m_{b\_modern,n} - \overline{m_{b\_modern}}\right)\frac{\partial Fm_{std}}{\partial m_{b\_modern}} + \left(m_{b\_dead,n} - \overline{m_{b\_dead}}\right)\frac{\partial Fm_{std}}{\partial m_{b\_dead}}\right]^2 \quad (10)$$

Multiplying out the summed part of Equation 10 would result in 10 terms, six of which represent covariance between the uncertainties in Fm and masses of the standard and process blanks. The covariance terms would all be zero if they were independent from each other, but the modern and dead components of the graphitization blank are not necessarily independent of each other in this case. So we reformulate Equation 8 to combine the modern and dead blank components into a single mass, m_b, and combined fraction modern, Fm_b, yielding:

$$Fm_{std} = \frac{m_{meas} * Fm_{meas} - m_b * Fm_b}{m_{meas} - m_b} \quad (11)$$

and

$$\sigma^2_{Fm_{std}} = \frac{1}{N}\sum_1^N f\left[\left(Fm_{meas,n} - \overline{Fm_{meas}}\right)\frac{\partial Fm_{std}}{\partial Fm_{meas}} + \left(m_{meas,n} - \overline{m_{meas}}\right)\frac{\partial Fm_{std}}{\partial m_{meas}} + \left(m_{b,n} - \overline{m_b}\right)\frac{\partial Fm_{std}}{\partial m_b}\right]^2 \quad (12)$$

or equivalently,

$$\sigma^2_{Fm_{std}} = \left(\frac{m_{meas}}{m_{meas} - m_b}\right)^2 \sigma^2_{Fm_{meas}} + \left(\frac{m_b * Fm_b - m_{meas} * Fm_b}{(m_{meas} - m_b)^2}\right)^2 \sigma^2_{m_{meas}} + \left(\frac{m_b}{m_{meas} - m_b}\right)^2 \sigma^2_{Fm_b} + \left(\frac{m_{meas} * Fm_{meas} - m_{meas} * Fm_b}{(m_{meas} - m_b)^2}\right)^2 \sigma^2_{m_b} \quad (13)$$

The square root of the variance, $\sigma^2_{Fm_{std}}$, according to Equation 13 was used to calculate the uncertainty in blank-corrected primary and secondary standards (Figure 9b). With a few exceptions, corrected fractions modern for targets produced by ultra-small reactors are within propagated uncertainty of their expected Fm values.

TEST STUDY: INDIVIDUAL FORAMINIFERA ANALYSIS

Keigwin and Guilderson (2009) demonstrated that the ^{14}C contents of planktonic foraminifera on the seafloor are affected by bioturbation with consequences for sediment dating and circulation studies. These authors suggest that measurements of individual foraminiferal tests would allow for the magnitude of the bioturbation effect to be investigated in different sedimentary settings. To demonstrate our ability to measure small numbers of foraminiferal tests, we analyzed live-stained and unstained benthic foraminifera (*Uvigerina*) from the sediment-water interface from the Sea of Okhotsk (Keigwin and Gagnon 2015) and compared the results with previously measured bulk ^{14}C dates (Figure 10). The bulk ^{14}C ages of stained (1530 ± 25 yr BP) and unstained (1770 ± 65 yr BP) tests were measured on 2.5 mg $CaCO_3$, or approximately 150 individual tests. All results shown in

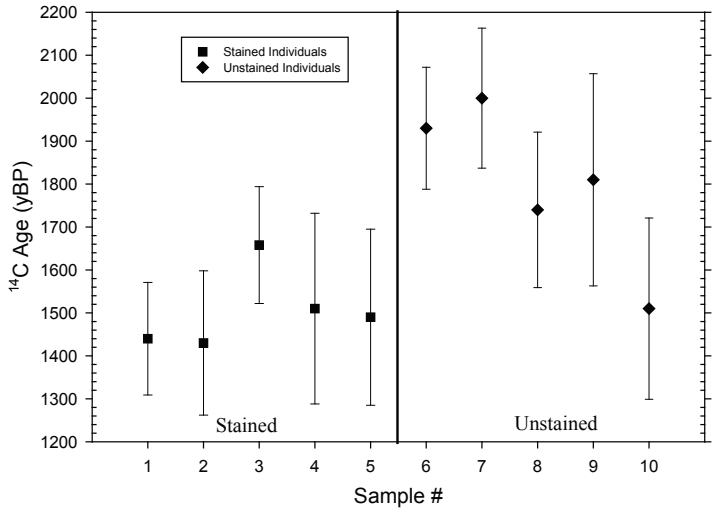

Figure 10 Comparison of ^{14}C dates for stained vs. unstained bulk and individual benthic foraminifera from the Sea of Okhotsk.

Figure 10 were corrected for both a hydrolysis and graphite process blank, utilizing the values expressed in this manuscript. There is reasonable agreement between small numbers (three individuals that generated 12 µg C) of stained foraminifera and the bulk ^{14}C age, yet greater variability with the unstained comparison results. This variability issue, along with procedures used and other details are specifically outlined in Keigwin and Gagnon (2015). Error bars on ultra-microscale samples are inflated due to the relatively low count rates measured on the samples before the graphite in each target was completely ionized. As a proof of concept, it appears this technique provides an avenue to further explore whether ^{14}C data from individual foraminifera can help unlock the mysteries of bioturbation in ocean sediment cores.

CONCLUSION

At the NOSAMS facility, we have developed ultra-small graphitization reactors with a nominal internal volume of 0.8 mL. These reactors, constructed of commercially available, 1/8″ diameter components, successfully graphitize samples in the range of 6–100 µg C. As reported by other laboratories (Hua et al. 2001; Santos et al. 2007), we observe an isotopic fractionation effect associated with converting small quantities of CO_2 to graphitic carbon, which is most prominent for samples containing less than 10 µg C. Although this effect indicates an incomplete graphitization reaction, the resulting targets can be successfully measured by CFAMS with a ^{13}C correction. Efforts to understand this effect and improve our reaction conditions continue. However, we do not see the same rapid collapse in beam current observed for small samples reported by other AMS facilities (Santos et al. 2007; Liebl et al. 2013), and instead appear to be trading off current yield for target longevity.

For a suite of primary and secondary standards spanning a range of Fm values, our measured Fm values are in good agreement with expected values for samples larger than 10 µg C (Figure 9a) but deviate for smaller samples. To correct for this deviation, we assumed the ultra-small graphitization reactors contribute a constant-mass blank, which we estimate to be 0.3 ± 0.1 µg C with an Fm value of 0.43 ± 0.3, and corrected for the blank contribution. Blank correction improves the agreement between measured and expected values to within uncertainty for most ultra-microscale samples (Figure 9b). We note, however, that blank correction does not bring some of the smallest samples into

agreement with expected values and acknowledge that other factors will contribute to these deviations from expected Fm values. Our attempts to include all influences by correcting ultra-microscale Fm values by normalization to small standards does not improve the agreement between measured and expected Fm values (Figure 8). Efforts to understand and correct for these factors continue.

ACKNOWLEDGMENTS

We are very grateful to Lloyd Keigwin who provided stained and unstained benthic foraminifera as well as bulk ^{14}C dates for our proof of concept. We are indebted to Bill Jenkins and Steve Beaupré for valuable discussions that improved the blank calculations described in this manuscript. We are also grateful to Pat Long for pressing the graphite into targets. This work was funded by the NSF Cooperative Agreement for the Operation of a National Ocean Sciences Accelerator Mass Spectrometry Facility (OCE-0753487). S R Shah Walter was also partially supported by the WHOI Postdoctoral Scholar Program.

REFERENCES

Currie LA, Polach HA. 1980. Exploratory analysis of the International Radiocarbon Cross-Calibration Data: consensus values and interlaboratory error. *Radiocarbon* 22(3):933–5.

Drenzek NJ, Montluçon DB, Yunker MB, Macdonald RW, Eglinton TI. 2007. Constraints on the origin of sedimentary organic carbon in the Beaufort Sea from coupled molecular ^{13}C and ^{14}C measurements. *Marine Chemistry* 103(1–2):146–62.

Gagnon AR, McNichol AP, Donoghue JC, Stuart DR, von Reden K, NOSAMS. 2000. The NOSAMS sample preparation laboratory in the next millenium: progress after the WOCE program. *Nuclear Instruments and Methods in Physics Research B* 172(1–4):409–15.

Hua Q, Jacobsen GE, Zoppi U, Lawson EM, Williams AA, Smith AM, McGann MJ. 2001. Progress in radiocarbon target preparation at the ANTARES AMS Centre. Radiocarbon 43(2A):275–82.

Hua Q, Zoppi U, Williams AA, Smith AM. 2004. Small-mass AMS radiocarbon analysis at ANTARES. *Nuclear Instruments and Methods in Physics Research B* 223–224:284–92.

Ingalls AE, Shah SR, Hansman RL, Aluwihare LI, Santos GM, Druffel ERM, Pearson A. 2006. Quantifying archaeal community autotrophy in the mesopelagic ocean using natural radiocarbon. *Proceedings of the National Academy of Sciences USA* 103(17):6442–7.

Ingalls AE, Ellis EE, Santos GM, McDuffee KE, Truxal L, Keil RG, Druffel ERM. 2010. HPLC purification of higher plant-dervied lignin phenols for compound specific radiocarbon analysis. *Analytical Chemistry* 82(21):8931–8.

Keigwin LD, Gagnon AR. 2015. Comparison of large and ultra-small $\Delta^{14}C$ measurements in core top benthic foraminifera from the Okhotsk Sea. *Radiocarbon* 57(1):123–8.

Keigwin LD, Guilderson TP. 2009. Bioturbation artifacts in zero-age sediments. *Paleoceanography* 24(4):PA4212, doi:10.1029/2008PA001727.

Kirner DL, Taylor RE, Southon JR. 1995. Reduction in backgrounds of microsamples for AMS ^{14}C dating. *Radiocarbon* 37(2):697–704.

Kitagawa H, Masuzawa T, Makamura T, Matsumoto E. 1993. A batch preparation method for graphite targets with low background for AMS ^{14}C measurements. *Radiocarbon* 35(2):295–300.

Le Clercq M, van der Plicht J, Gröning M. 1998. New ^{14}C reference materials with activities of 15 and 50 pMC. *Radiocarbon* 40(1):295–7.

Liebl J, Ortiz RA, Golser R, Handle F, Kutschera W, Steier P, Wild EM. 2010. Studies on the preparation of small ^{14}C samples with an RGA and ^{13}C-enriched material. *Radiocarbon* 52(3):1394–404.

Liebl J, Steier P, Golser R, Kutschera W, Mair K, Priller A, Vonderhaid I, Wild EM. 2013. Carbon background and ionization yield of an AMS system during ^{14}C measurements of microgram-size graphite samples. *Nuclear Instruments and Methods in Physics Research B* 294:335–9.

Mann WB. 1983. An international reference material for radiocarbon dating. *Radiocarbon* 25(2):519–27.

McNichol AP, Gagnon AR, Jones GA, Osborne EA. 1992. Illumination of a black box: analysis of gas composition during graphite target preparation. *Radiocarbon* 34(3):321–9.

Ohkouchi N, Eglinton TI, Keigwin LD, Hayes JM. 2002. Spatial and temporal offsets between proxy records in a sediment drift. *Science* 298(5596):1224–7.

Ohkouchi N, Xu L, Reddy CM, Montluçon D, Eglinton TI. 2005. Radiocarbon dating of alkenones from marine sediments: I. isolation protocol. *Radiocarbon* 47(3):401–412.

Osborne EA, McNichol AP, Gagnon AR, Hutton DL, Jones GA. 2000. Internal and external checks in the NOSAMS sample preparation laboratory for target quality and homogeneity. *Nuclear Instruments and Methods in Physics Research B* 92(1–4):158–61.

Pearson A, McNichol AP, Schneider RJ, von Reden KF. 1998. Microscale AMS ^{14}C measurement at NOSAMS. *Radiocarbon* 40(1):61–75.

Pearson A, Seewald JS, Eglinton TI. 2005. Bacterial incorporation of relict carbon in the hydrothermal environment of Guaymas Basin. *Geochimica et Cosmochimica Act*a 69(23):5477–86.

Roberts ML, Burton JR, Elder KL, Longworth BE, McIntyre CP, von Reden KF, Han BX, Rosenheim BE, Jenkins WJ, Galutschek E, McNichol AP. 2010. A high-performance ^{14}C accelerator mass spectrometry system. *Radiocarbon* 52(2):228–35.

Rosenheim BE, Galy V. 2012. Direct measurement of riverine particulate organic carbon age structure. *Geophysical Research Letters* 39:L198703, doi:10.1029/2012GL052883.

Rosenheim BE, Day MB, Domack E, Schrum H, Benthien A, Hayes JM. 2008. Antarctic sediment chronology by programmed-temperature pyrolysis: methodology and data treatment. *Geochemistry, Geophysics, Geosystems* 9:Q04005, doi:10.1029/2007GC001816.

Rozanski K, Stichler W, Gonfiantini R, Scott EM, Beukens RP, Kromer B, van der Plicht J. 1992. The IAEA ^{14}C intercomparison exercise 1990. *Radiocarbon* 34(3):506–19.

Santos GM, Southon JR, Griffin S, Beaupré SR, Druffel ERM. 2007. Ultra small-mass AMS ^{14}C sample preparation and analyses at KCCAMS/UCI Facility. *Nuclear Instruments and Methods in Physics Research B* 259(1):293–302.

Santos GM, Southon JR, Drenzek NJ, Ziolkowski LA, Druffel ERM, Xu X, Zhang D, Trumbore S, Eglinton TI, Hughen KA. 2010. Blank assessment for ultra-small radiocarbon samples: chemical extraction and separation versus AMS. *Radiocarbon* 52(3):1322–35.

Scott EM. 2003. The Third International Radiocarbon Intercomparison (TIRI) and the Fourth International Radiocarbon Intercomparison (FIRI): Section 10. *Radiocarbon* 45(2):285–90.

Shah SR, Pearson A. 2007. Ultra-microscale (5–25 μg C) analysis of individual lipids by ^{14}C AMS: assessment and correction for sample processing blanks. *Radiocarbon* 49(1):69–82.

Stuiver M. 1983. International agreements and the use of the new oxalic acid standard. *Radiocarbon* 25(2):793–5.

Stuiver M, Polach HA. 1977. Discussion: reporting of ^{14}C data. *Radiocarbon* 19(3):355–63.

van der Borg K, Alderliesten C, de Jong AFM, van den Brink A, de Haas AP, Kersemaekers HJH, Raaymakers JEMJ. 1997. Precision and mass fractionation in ^{14}C analysis with AMS. *Nuclear Instruments and Methods in Physics Research B* 123(1–4):97–101.

Verkouteren RM, Klinedinst DB, Currie LA. 1997. Iron-manganese system for preparation of radiocarbon AMS targets: characterization of precedural chemical-isotopic blanks and fractionation. *Radiocarbon* 39(3):269–83.

Vogel JS, Nelson DE, Southon JR. 1987. ^{14}C background levels in an accelerator mass spectrometry system. *Radiocarbon* 29(3):323–33.

von Reden KF, McNichol AP, Pearson A, Schneider RJ. 1998. ^{14}C AMS measurements of <100 μg samples with a high-current system. *Radiocarbon* 40(1):247–53.

Xu X, Trumbore SE, Zheng S, Southon JR, McDuffee KE, Luttgen M, Liu JC. 2007. Modifying a sealed tube zinc reduction method for preparation of AMS graphite targests: reducing background and attaining high precision. *Nuclear Instruments and Methods in Physics Research B* 259(1):320–9.

Yokoyama Y, Koizumi M, Matsuzaki H, Miyairi Y, Ohkouchi N. 2010. Developing ultra small-scale radiocarbon sample measurement at the University of Tokyo. *Radiocarbon* 52(2):310–8.

Ziolkowski LA, Druffel ERM. 2009. Quantification of extraneous carbon during compound specific radiocarbon analysis of black carbon. *Analytical Chemistry* 81(24):10,156–61.